# OPTIMIZATION OF ROTATIONAL OIL-SPRAY-COOLING STRUCTURE AND TEMPERATURE FIELD ANALYSIS OF PMSM IN VEHICLE

***Chen YANG*, Wei CAI and Baicheng SHAO***

School of Electrical and Electronic Engineering, Harbin University of Science and Technology, Harbin, China

* Corresponding author; E-mail: yangchen5526@163.com

*The heat dissipation of the permanent magnet synchronous motor (PMSM) of an electric vehicle is always worthy of attention, and the design of the cooling system of the PMSM is very important. The rotor rotational oil-spray-cooling structure is widely used in PMSM with hairpin winding. The oil enters from one side of the hollow shaft and is sprayed from the outlets of the front and rear, respectively, which realizes the cooling of the winding at both ends. However, the flow difference on both sides of the shaft will cause the problem of uneven cooling of the winding and the issue of local overheating of the motor. Therefore, the hollow shaft structure needs to be optimized. A 120 kW oil-cooled motor is analyzed as an example in this paper. The flow field distribution during the rotation of the rotor and the reasons for the uneven shunt are analyzed. And the structural parameters of the hollow shaft are optimized by using the Taguchi method and the response surface method. It was found that the new shaft structure can better realize the shunt and reduce the winding and rotor temperature. It provides a guide for the design of the rotational oil-spray-cooling structure of the oil-cooling PMSM.*

Key words*: oil-cooling PMSM, temperature field, fluid field, structure optimization*

## 1. Introduction

With the strengthening of environmental awareness, energy vehicles have developed rapidly in recent years. Permanent magnet synchronous motor (PMSM) has become the first choice for electric vehicles because of its high power density, high torque density and wide speed control range [1-2]. However, if the motor temperature exceeds the limit, it will affect the normal operation of the motor, and even lead to permanent magnet demagnetization [3]. Therefore, the cooling system is critical to ensuring the normal operation of the motor.

The cooling systems of PMSM for vehicles include the water-cooling system and the oil-cooling system. At present, many scholars have studied the cooling performance of the water-cooling structures. The water-cooling pipe is placed on the stator yoke to reduce the stator temperature [4]. The structural parameters and water channel shape have been optimized to reduce the motor temperature [5]. Because water cannot come into direct contact with the winding, the water cooling system is insufficient for cooling the motor with the hairpin winding. Therefore, more and more scholars are paying attention to the oil-cooling system. Many oil-supplied parameters are analyzed to

improve the oil-cooling performance of the end winding of the electric machines [6]. A calculation model to predict the convective heat transfer coefficient for the oil spray cooling hairpin winding is proposed in [7]. However, the flow difference on both sides of the shaft will cause the problem of uneven cooling of the winding on both sides which is a common problem in oil cooling systems. In order to solve this problem, a new oil injection cooling structure which opens an oil channel in the rotor core is proposed in [8]. However, it causes additional processing costs. As a result, this work proposes directly optimizing the structure of the hollow shaft, which is both easy to manufacture and maintains the electromagnetic performance of the motor.

At present, the main methods for studying the cooling performance of motors are divided into computational fluid dynamics (CFD) and lumped parametric thermal networks (LPTN). A thermal network model is proposed to predict the motor temperature rise accurately [9]. The synergized lumped-parameter and sub-domain thermal models for the track of the hotspots of the motor is studied in [10]. With the development of computer technology, the CFD and finite element methods (FEM) are more and more applied to the calculation of motor cooling performance. The CFD simulation model for the water-cooling PMSM is built to calculate the temperature field in [11]. The coolant distribution and heat transfer in the electric drive unit is analyzed by the CFD model [12-13]. Therfore, CFD and FEM can accurately calculate the fluid field and temperature filed, which is useful for studying the oil distribution of oil-cooled motors. This paper uses CFD and FEM to analyze the fluid field and temperature field of the oil-cooling motor and optimize the rotating shaft structure.

There are many kinds of methods to optimize the structure, such as the genetic algorithm [14,15], the particle swarm optimization algorithm [16], the Taguchi orthogonal algorithm [17] and the response surface method [18]. But for optimizations with a small number of optimization parameters, the Taguchi orthogonal algorithm and the response surface method are combined to carry out multi-objective optimization. This combation method has a short solution time and uses the least number of experiments to complete the optimization of the shaft structure in this paper.

The novelty of this work is that it solved the issue of uneven cooling on both end windings by optimizing the structure of the hollow shaft, which is applicable to the oil-cooling motor with the rotational oil-spray-cooling structure. The harm caused by the uneven flow of the hollow shaft is analyzed by calculating the temperature field of the motor. The hollow shaft structure is optimized by the Taguchi method and the response surface method. The relationship between the shaft parameters and the optimization objective is established. By comparing the flow field and temperature field before and after optimization, the problem of uneven cooling is solved. It provides guidance for the design of an oil-cooling system for the PMSM with a rotational oil-spray-cooling structure.

## 2. Model of motor and CFD setting

### 2.1. Main parameters and mathematical model

Fig. 1(a) shows the fluid-solid coupling model of the oil-cooled PMSM with hairpin winding used in this paper, and the main parameters of the motor are shown in Tab. 1. The rated power is 120 kW and the rated speed is 8000 rpm. The cooling system of this motor is water-oil mixture cooling, including water channel on the frame and oil-cooling structure. The fluid domain includes the water, oil and air. When the motor runs at high speed, the oil enters the hollow shaft from the inlet, and some of the oil exits through outlet 1 due to the centrifugal force and pressure. The other oil flows to outlet 2,

where it is discharged. Because most of the oil flows out of outlet 1, the pressure is reduced. Therefore, the mass flow rate of outlet 1 is significantly greater than that of outlet 2. The mass flow rate difference at two outlets of the shaft has a direct impact on the cooling of the end winding. It results in unequal cooling and localized overheating of the motor. The paths that rotor uses to dissipate heat are shown in Fig. 1(b). The heat generated by the rotor is dissipated through the air gap as well as cooled by the oil flowing in the shaft. When most oil flows away from outlet 1, the mass flow rate of oil flowing in the shaft is reduced. Therefore, the rotor cannot be cooled by oil, resulting in the temperature of the permanent magnet rising. It is very important to optimize the structure of the shaft and balance the mass flow rate difference between the both sides.

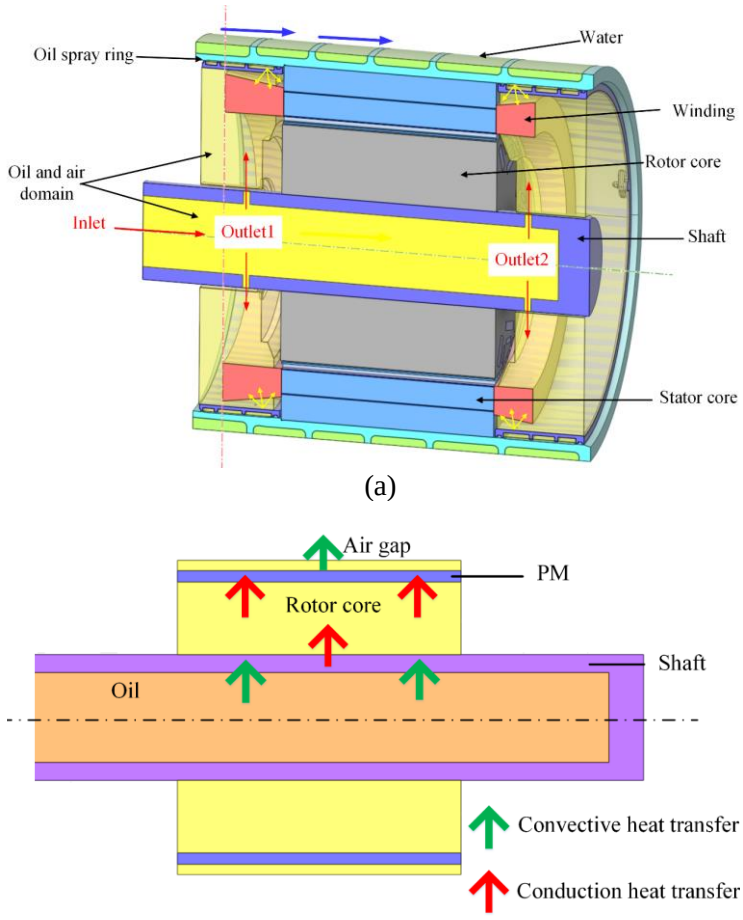


**Fig. 1. (a) The fluid-solid coupling model of the oil-cooled PMSM with hairpin winding. (b) The paths that rotor uses to dissipate heat.**

**Table 1. Main parameters of PMSM.**

| Parameters | Values | Parameters | Values |
|---|---|---|---|
| Rated power | 120 kW | Outer stator diameter | 220mm |
| Rated speed | 8000 rpm | Inner stator diameter | 148mm |
| Number of phases | 3 | Axial length | 130mm |
| Slots/ poles | 48/8 | Air gap | 0.8mm |

In order to analyze the cooling performance of the rotor rotational oil-spray-cooling structure, it is necessary to calculate the fluid field and temperature field of the motor. The three-dimensional fluid-solid coupling solution model of motor is established, and the temperature of the motor is calculated by the finite element method in this paper. Because the velocity is much less than the speed of sound and they are regarded as incompressible fluids. There are many methods for the calculation of the motor fluid field, including the SST model, the *k*-*ε* model, and the *k*-*w* model. The standard *k*-ε model is suitable for incompressible fluid viscosity simulation. And the standard *k*-ε model has good convergence and a small amount of calculation. Therefore, the standard *k*-ε model is used to calculate the fluid field in this paper. And the equation is as follows [19]:

$$\begin{cases} \dfrac{\partial}{\partial t}(\rho k)+\nabla\cdot(\rho k\boldsymbol{u})=\nabla\cdot[(\mu+\dfrac{\mu_t}{\sigma_k})\nabla k]+G_k-\rho\varepsilon \\ \dfrac{\partial}{\partial t}(\rho\varepsilon)+\nabla\cdot(\rho\boldsymbol{u}\varepsilon)=\nabla\cdot[(\mu+\dfrac{\mu_t}{\sigma_\varepsilon})\nabla\varepsilon]+G_{1\varepsilon}\dfrac{\varepsilon}{k}G_k-G_{2\varepsilon}\rho\dfrac{\varepsilon^2}{k} \end{cases} \tag{1}$$

where $k$ is the turbulence kinetic energy, $\varepsilon$ is the dissipation rate, $\sigma_k$, $\sigma_\varepsilon$, $G_{1\varepsilon}$, $G_{2\varepsilon}$ are constants, and $G_k$ is turbulence kinetic term associated with the mean velocity gradient.

In the calculation of the three-dimensional transient temperature field for anisotropic materials, the expression of the transient heat conduction differential equation in the solution domain is as follows [20]:

$$\begin{cases} \dfrac{\partial}{\partial x}(\lambda_x\dfrac{\partial T}{\partial x})+\dfrac{\partial}{\partial y}(\lambda_y\dfrac{\partial T}{\partial y})+\dfrac{\partial}{\partial z}(\lambda_z\dfrac{\partial T}{\partial z})+q_v=\rho c\dfrac{\partial T}{\partial t} \\ T\big|_{s_1}=T_w \\ -\boldsymbol{\lambda}\dfrac{\partial T}{\partial \boldsymbol{n}}\Big|_{s_2}=q_w \\ \boldsymbol{\lambda}\dfrac{\partial T}{\partial \boldsymbol{n}}\Big|_{s_3}=-h(T-T_f) \end{cases} \tag{2}$$

where $\lambda_x$, $\lambda_y$, $\lambda_z$ is the thermal conductivity of solid materials along different directions, W/(m·°C); $T$ is the temperature of the boundary surface, °C; $q_v$ is the heat flux of internal heat source, W/m$^3$; $\rho$ is the density, kg/m$^3$; $c$ is the specific heat capacity, J/(kg·°C); $s_1$, $s_2$ and $s_3$ are boundaries; $n$ is the normal vector of the surface to be evaluated. $T_w$ is the boundary temperature, °C; $T_f$ is the fluid temperature, °C; $t$ is the time term, $s$; $q_w$ is the boundary heat flux, W/m$^3$; $h$ is the convective heat transfer coefficient, W/(m$^2$·°C).

In this paper, the method of volume of fluid (VOF) is used to solve the multiphase flow. For the phase of $q$, the continuity equation of the VOF method is as follows [21]:

$$\frac{\partial \alpha_q}{\partial t}+\nabla\cdot(\alpha_q\rho_q v_q)=0 \tag{3}$$

$$\alpha_{\text{oil}}+\alpha_{\text{air}}=1 \tag{4}$$

where $\rho_q$ is the density, $v_q$ is the velocity, and $\alpha_q$ is the volume fraction of the phase of $q$. $\alpha_{\text{oil}}$ is the volume fraction of the phase of oil. $\alpha_{\text{air}}$ is the volume fraction of the phase of air. The sum of the oil and air volume fraction is 1 in each grid in the VOF method. If $\alpha_{\text{oil}} = 0$, there is no oil in this grid. If $0 < \alpha_{\text{oil}} < 1$, there is both oil and air in this grid. If $\alpha_{\text{oil}} = 1$, there is no air in this grid.

### 2.2. Boundary conditions and assumptions

In order to simplify the calculation, all insulating materials in the slot are equivalent to an insulating layer close to the wall of the slot [22]. The air gap is equivalent to the solid, and its thermal conductivity is calculated according to the method in reference [22]. And the fluid-solid coupling model is shown in Fig. 1(a). The solid domain includes the casing, stator core, rotor core, winding, permanent magnet and rotating shaft. The fluid domain includes an oil-air mixed domain and a spiral water domain. The basic assumptions and boundary conditions of the three-dimensional temperature field of the motor are as follows. The internal heat transfer of the motor only considers heat conduction and heat convection, ignoring the influence of heat radiation on the temperature rise of the motor. The contact surface between solid and fluid is set as the non-slip contact surface. The ambient temperature of the motor is 65 ℃. The inlet oil temperature is 75 °C and the flow rate is 4.3 L/min. The outlet pressure of the fluid domain is zero. The material parameters and heat density distribution of each region of the motor are set. The material parameters of the motor are shown in Tab. 2, and the heat density distribution of each region of the motor is shown in Tab. 3.

**Table 2. Material parameters of the motor**

| Parameters | Thermal conductivity(W/(m·K)) | Density(kg/m³) | Specific heat capacity(J/(kg·K)) |
|---|---|---|---|
| Stator and rotor core | 28(Radial) 6(Axial) | 7750 | 460 |
| Winding | 388 | 8933 | 385 |
| Insulation | 0.17 | 1700 | 1420 |
| PM | 7.6 | 7500 | 460 |
| Shaft | 49.8 | 7800 | 448 |
| Shell | 128 | 2790 | 833 |

**Table 3. Heat source of the motor**

| | Winding in slot | End winding | Stator core | Rotor core | PM |
|---|---|---|---|---|---|
| Heat source ($W/m^3$) | 2.45e6 | 8.95e5 | 7.52e5 | 3.47e5 | 6.91e4 |

### 2.3. Model verification

In order to ensure the accuracy of the calculation, the grid independence is verified. The mass flow of two outlets under different grid numbers of the fluid domain in the hollow shaft is calculated, and the results are shown in Fig. 2. The error of the flow rate of outlet 1 ($Q_1$) is 2.59% and the error of the flow rate of outlet 2 ($Q_2$) is 2.13% between the 0.29 million grids and the 0.79 million grids. When the number of grids is 0.29 million, the calculation results are independent of the grid density. After calculation, the value of y+ (the dimensionless parameter of the first mesh thickness) is 22, which meets the requirement of the $k$-$\varepsilon$ equation for mesh quality in the calculation process [23]. The same method is used to verify the grid independence of the 3D fluid-solid temperature field model of the motor, and the number of grids in the whole motor model is 4.22 million.

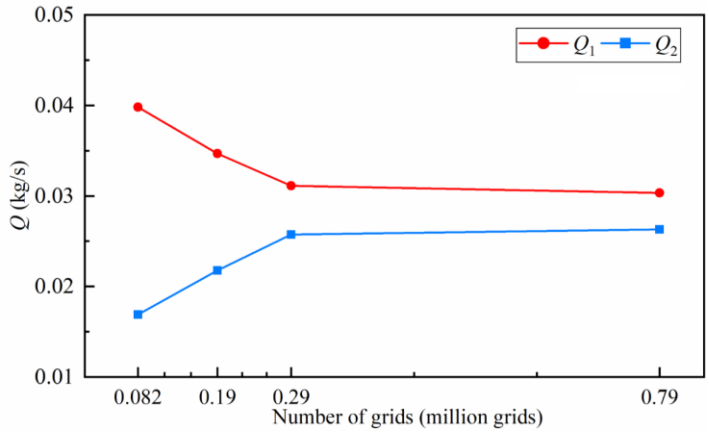


**Fig. 2. Verification of grid independence.**

## 3. Hollow shaft optimized and optimization method

### 3.1. Optimization method

Considering the calculation accuracy and optimization period, the combination of the Taguchi method and the response surface method is used to optimize the hollow shaft structure, and the process of optimization is shown in Fig. 3. Firstly, the optimization parameters and optimization objectives are determined, and the Taguchi orthogonal method is carried out to determine the influence of the optimization parameters on various optimization objectives. For the unimportant parameters, the parameters are directly determined by the results of the Taguchi method. For the important parameters, the response surface method (RSM) is used to determine the effect trend of the optimization parameters on the optimization objective and determine the optimal parameter combination. Finally, the optimization effectiveness is analyzed by comparing the temperature field of the motor.

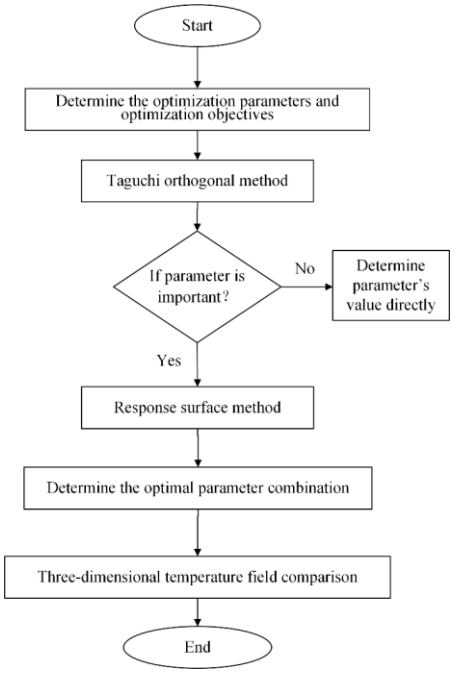


**Fig. 3. Process of optimization.**

### 3.2. Taguchi orthogonal method

The optimization parameters affecting the oil flow difference of the shaft are as follows: A (the radius of the outlet 1), B (the radius of the outlet 2), C (the inner radius of the shaft), D (the angle between the center line of the outlet and the vertical axis of the outlets), and E (the number of holes in the unilateral outlets), as shown in Fig. 4. In order to ensure the structural symmetry and dynamic balance characteristics of the rotor, the parameters of each outlet on the same side are completely the same. The level values of the optimization parameters are determined as shown in Tab. 4, considering the requirements of mechanical strength.

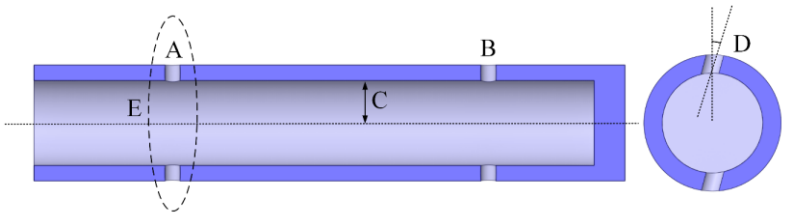


**Fig. 4. Hollow shaft structure and optimization parameters.**

**Table 4. Optimization parameters and level values.**

| | A (mm) | B (mm) | C(mm) | D(°) | E |
|---|---|---|---|---|---|
| Level 1 | 2 | 2 | 16 | 0 | 2 |
| Level 2 | 3 | 3 | 20 | 7.5 | 3 |
| Level 3 | 4 | 4 | 24 | 15 | 4 |

In order to ensure the cooling performance of the rotor and winding, the following variables are determined as optimization objectives: $T_{max}$ (the maximum temperature of the PM), $T_{diff}$ (the temperature difference of the PM), $Q_{diff}$ (the relative difference of the mass flow rate on outlet 1 and outlet 2), $P$ (the pressure difference inside the shaft). $T_{diff}$ and $Q_{diff}$ are calculated as follows:

$$T_{diff} = T_{max} - T_{min} \tag{5}$$

$$Q_{diff} = \left| \frac{Q_1 - Q_2}{Q} \right| \times 100\% \tag{6}$$

where $T_{min}$ is the minimum temperature of PM, ℃; $Q$ is the total mass flow rate of inlet, *g/s*; $Q_1$ and $Q_2$ are the mass flow rates of outlet 1 and outlet 2, respectively, g/s.

According to the calculation criterion of the Taguchi method, an orthogonal experimental design is carried out. A five-factor, three-level orthogonal matrix is established. Eighteen experiments were carried out. The finite element method is used to calculate the fluid field and temperature field, and the simulation results are shown in Tab. 5.

**Table 5. Taguchi orthogonal table.**

| Number | Optimization parameters | | | | | Simulation results | | | |
|---|---|---|---|---|---|---|---|---|---|
| | A | B | C | D | E | $T_{max}$/℃ | $T_{diff}$/℃ | $Q_{diff}$/% | $P$/kPa |
| 1 | 1 | 1 | 1 | 1 | 1 | 109.73 | 6.05 | 10.18 | 30.26 |
| 2 | 1 | 2 | 2 | 2 | 2 | 107.21 | 5.64 | 9.86 | 29.77 |
| 3 | 1 | 3 | 3 | 3 | 3 | 110.79 | 5.30 | 80.23 | 38.49 |
| 4 | 2 | 1 | 1 | 2 | 2 | 109.42 | 6.02 | 42.88 | 77.05 |
| 5 | 2 | 2 | 2 | 3 | 3 | 112.41 | 5.50 | 90.37 | 44.35 |

| | | | | | | | | | |
|---|---|---|---|---|---|---|---|---|---|
| 6 | 2 | 3 | 3 | 1 | 1 | 106.26 | 5.49 | 17.71 | 50.13 |
| 7 | 3 | 1 | 2 | 1 | 3 | 108.69 | 5.51 | 78.88 | 16.89 |
| 8 | 3 | 2 | 3 | 2 | 1 | 109.26 | 5.44 | 100.00 | 39.74 |
| 9 | 3 | 3 | 1 | 3 | 2 | 199.02 | 9.82 | 100.00 | 28.46 |
| 10 | 1 | 1 | 3 | 3 | 2 | 118.07 | 5.75 | 100.00 | 51.71 |
| 11 | 1 | 2 | 1 | 1 | 3 | 110.33 | 5.59 | 93.21 | 87.06 |
| 12 | 1 | 3 | 2 | 2 | 1 | 107.25 | 5.62 | 95.45 | 48.58 |
| 13 | 2 | 1 | 2 | 3 | 1 | 107.29 | 5.75 | 36.79 | 28.98 |
| 14 | 2 | 2 | 3 | 1 | 2 | 106.66 | 5.53 | 38.76 | 24.76 |
| 15 | 2 | 3 | 1 | 2 | 3 | 111.19 | 5.25 | 81.16 | 20.07 |
| 16 | 3 | 1 | 3 | 2 | 3 | 108.49 | 5.55 | 83.24 | 37.95 |
| 17 | 3 | 2 | 1 | 3 | 1 | 147.54 | 16.16 | 100.00 | 36.95 |
| 18 | 3 | 3 | 2 | 1 | 2 | 108.52 | 5.27 | 52.22 | 23.25 |

Taking the calculation of the average value ($m$) of the optimization objective ($T_{max}$) under the parameter (A) at level 1 as an example. As shown in Formula (7), the average value of each optimization objective under each level of optimization parameters is shown in Fig. 5.

$$m_A(T_{max}) = \frac{1}{6}\sum_{i=1}^{6} T_{max}(i) \tag{7}$$

where $T_{max}(i)$ is the maximum temperature of PM in the ith simulation of the parameter A at level 1.

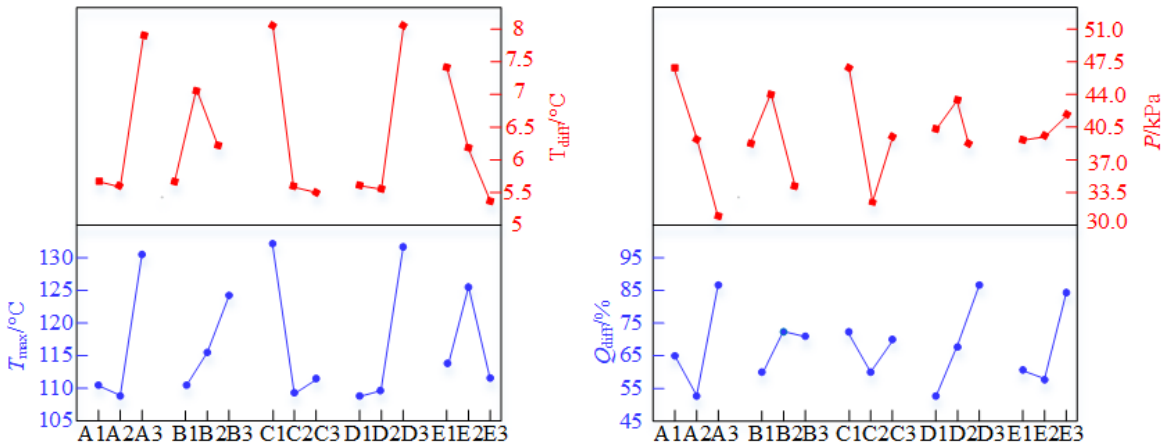


(a) (b)

**Fig. 5 The average value of the optimization objective at each level value.**

According to the calculation results of the average value in Fig. 5, it can be seen that the parameter combination with the minimum $T_{max}$ is A(2), B(1), C(2), D(1), E(3), the parameter combination with the minimum $T_{diff}$ is A(2), B(1), C(3), D(2), E(3), the parameter combination with the minimum $Q_{diff}$ is A(2), B(1), C(2), D(1), E(2) and the parameter combination with the minimum $P$ is A(3), B(3), C(2), D(3), E(1). The relative importance of the influence of each level factor on each optimization objective can be obtained by variance analysis. Taking the variance calculation of parameter A on $T_{max}$ as an example, as shown in Formula (8), the influence proportion of each optimization parameter on the optimization objective is calculated and shown in Tab. 6.

$$SS = \frac{1}{3}\sum_{i=1}^{3}(m_A(T_{max}(i)) - m(T_{max}))^2 \tag{8}$$

where $SS$ is the variance value, $m_A$ ($T_{max}$ ($i$)) is the average value of $T_{max}$ of parameter A at level $i$, m ($T_{max}$) is the average value of $T_{max}$.

According to the calculation results of variance, the influence proportion is analyzed. A higher variance means that the parameter has a greater impact on the optimization objective than other parameters. For $T_{max}$, the proportion of influence of each parameter from large to small is DCAEB. For $T_{diff}$, the order is CDAEB. For $Q_{diff}$, the order is DAEBC. For $P$, the order is ACBDE. Therefore, for each optimization objective, the influence ratio of parameters A, C and D is greater than that of B and E. The parameters A, C and D which have a significant influence, need to be optimized in the next step. According to the analysis results of the average value and variance, it can be concluded that the proportion of the influence of B on $P$ is higher than that of other optimization objectives. Therefore, according to the calculation results of the average value, the value of B corresponding to the minimum pressure difference is selected as 4 mm. The influence proportion of E on the flow difference $Q_{diff}$ is higher than that of other optimization objectives, the level value of E corresponding to the minimum flow difference $Q_{diff}$ is selected, which is 3.

**Table 6. Variance and proportion at various parameters.**

| | $T_{max}$ | | $T_{diff}$ | | $Q_{diff}$ | | $P$ | |
|---|---|---|---|---|---|---|---|---|
| | *SS* | Proportion/ % | *SS* | Proportion/ % | *SS* | Proportion/ % | *SS* | Proportion/% |
| A | 94.2 | 23.7 | 1.2 | 24.0 | 200.8 | 31.7 | 49.5 | 48.2 |
| B | 31.1 | 7.8 | 0.4 | 8.0 | 37.2 | 5.9 | 13.6 | 13.2 |
| C | 107.5 | 27.1 | 1.5 | 30.0 | 22.6 | 3.6 | 36.2 | 35.2 |
| D | 126.8 | 32.0 | 1.3 | 26.0 | 222.1 | 35.1 | 2.9 | 2.8 |
| E | 37.1 | 9.4 | 0.6 | 12.0 | 149.9 | 23.7 | 0.6 | 0.6 |
| total | 396.7 | 100.0 | 5.0 | 100.0 | 632.6 | 100.0 | 102.8 | 100.0 |

### 3.3. Response surface method

In order to optimize the important parameters A, C and D, it is necessary to use the response surface method to obtain the influence trend of the optimization parameters on the optimization objective, and then obtain the best combination of parameters. The response surface method mainly includes Central Composite Design (CCD) and Box-Behnken Design (BBD). BBD is more suitable for experiments with 2-5 parameters, and BBD requires fewer experiments with the same number of parameters compared with CCD. Therefore, this experiment was designed using the BBD method. Tab. 7 lists the level value of each optimization parameter, specifically, the three levels of each parameter are coded as -1, 0, 1, where 0 is the center point, 1 and -1 are relatively high and low values. Seventeen experiments were carried out, and the response surface was determined and shown in Fig. 6.

**Table 7. Level values of parameters at RSM.**

| Optimization parameters | Levels | | |
|---|---|---|---|
| | -1 | 0 | 1 |
| A(mm) | 2 | 3 | 4 |
| C(mm) | 16 | 20 | 24 |
| D(°) | 0 | 7.5 | 15 |

It can be seen from Fig. 6 that the slope of the outlet (D) and the inner radius of the shaft (C) have a great influence on the maximum temperature ($T_{max}$) of the PM, and they are positively

correlated with the $T_{max}$. The radius of outlet 1 (A) and the slope of the outlet (D) are positively correlated with the temperature difference of the permanent magnet ($T_{diff}$). Compared with C, A and D have a greater impact on $T_{diff}$. The radius of outlet 1 (A) and the slope of the outlet (D) have a great influence on the flow difference ($Q_{diff}$). And $Q_{diff}$ changes in the form of a parabola with the increase of A and D. The $Q_{diff}$ is the smallest when A is 2 mm and D is 7.5°. The pressure difference ($P$) is mainly related to the radius of outlet 1 (A) and the inner radius of the shaft (C), and they are negatively correlated with the pressure difference. Considering the influence of the inner radius of the shaft on the maximum temperature and pressure difference, the middle value of C should be 20 mm. The combination to determine the optimization parameters is shown in Tab. 8.

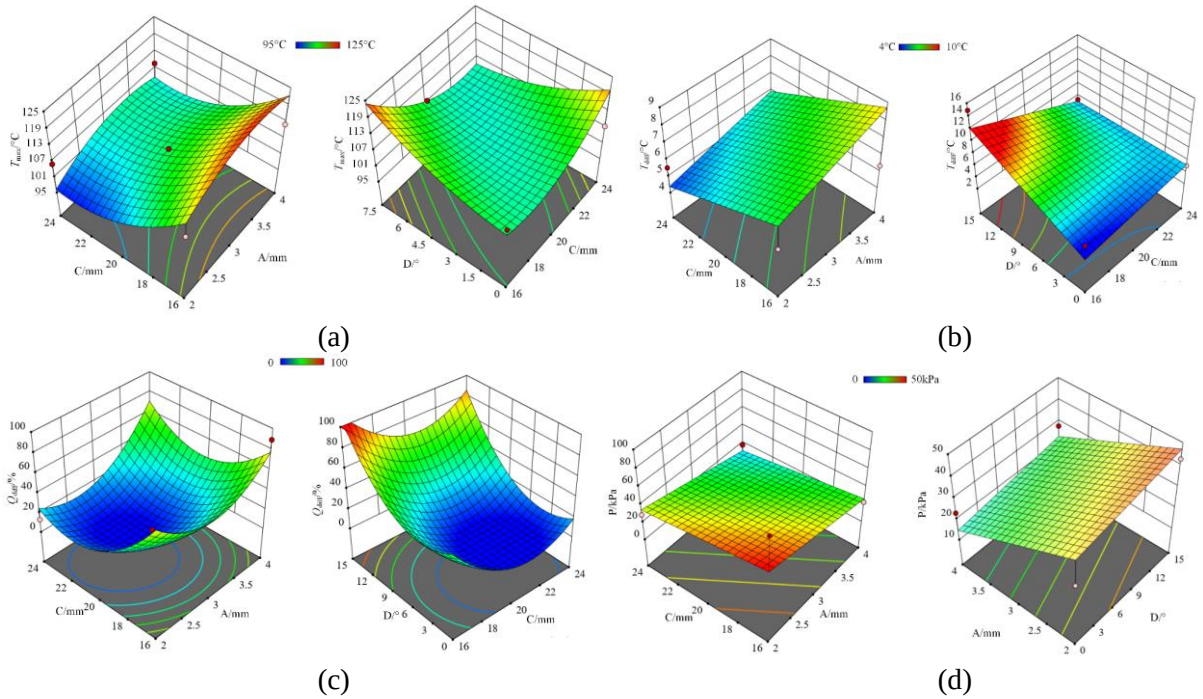


**Fig. 6 Response surface results. (a) $T_{max}$. (b) $T_{diff}$. (c) $Q_{diff}$. (d) $P$.**

**Table 8. Optimization parameters combination.**

| | A (mm) | B (mm) | C(mm) | D(°) | E |
|---|---|---|---|---|---|
| Optimization values | 2 | 4 | 20 | 7.5 | 3 |

## 4. Analysis and comparison of fluid field and temperature field

In order to compare the change in cooling performance before and after optimization, motors before and after optimization are modeled. The fluid field and temperature field are calculated. The oil volume fraction of the initial model (IM) and the optimization model (OM) at the rated working condition is shown in Fig. 7. It can be seen that the flow distribution at both ends of the motor is not uniform in Fig. 7(a), and the oil is thrown out to the winding from the outlet 1, but it cannot flow to the oil outlet 2. After optimization, as shown in Fig. 7(b), oil can achieve both ends of the winding flow, and cool the rotor. Therefore, oil is distributed in the motor cavities on the left and right sides.

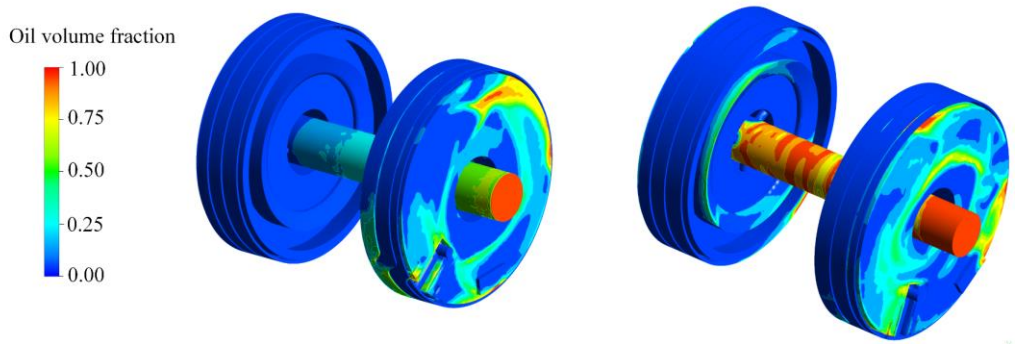


(a) (b)

**Fig. 7 Oil volume fraction distribution (a) Initial model (IM). (b) Optimization model (OM).**

The temperature field of the initial model and the optimization model at the rated working condition is shown in Fig. 8. Before optimization, the highest temperature of the motor appears on the rotor, and the temperature of the permanent magnet and the rotor core reaches 108.6 °C. There is a large temperature difference in the whole winding, and the temperature difference is up to 10 °C. This is because the oil is thrown out of outlet 1, and it cannot flow to outlet 2. And the winding at the back end cannot be cooled, resulting in a large temperature difference. At the same time, the rotor cannot be cooled by the oil. The rotor runs at a high speed of 8000 rpm, and the mechanical loss and eddy current loss generated by the rotor cannot be cooled by oil, and can only be cooled by the air gap, resulting in serious heating of the inner permanent magnet.

After the optimization of the motor, the maximum temperature of the winding is reduced, and the overall temperature difference is reduced by 2 °C, but the reduction is not large. Because when the oil flows through the shaft, it undergoes convective heat transfer with the rotor, resulting in a rise in the oil temperature. When the heated oil cools the winding at outlet 2, the cooling performance is reduced. The temperature of the rotor of the optimized motor is significantly reduced. And the maximum temperature is reduced from 108.6 °C to 105.6 °C, which indicates that the oil inside the shaft has a significant cooling performance on the rotor core and permanent magnet. After the comparison of the three-dimensional temperature field, the temperature rise of the optimized motor is significantly reduced in the rotor and winding under the same oil supply condition, which indicates the effectiveness of the optimization method.

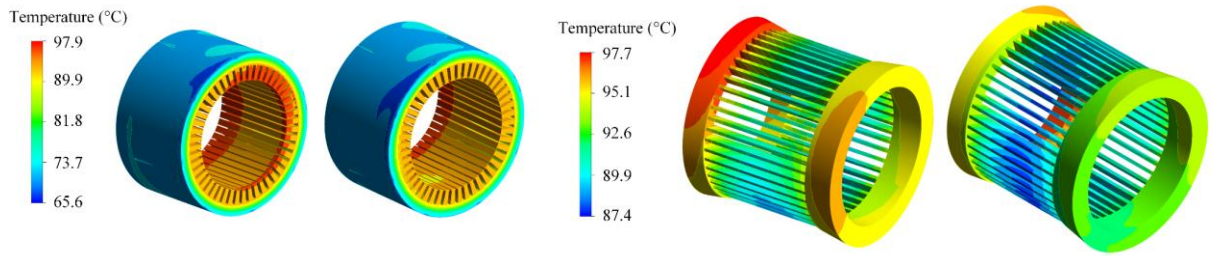


(a) (b) (c) (d)

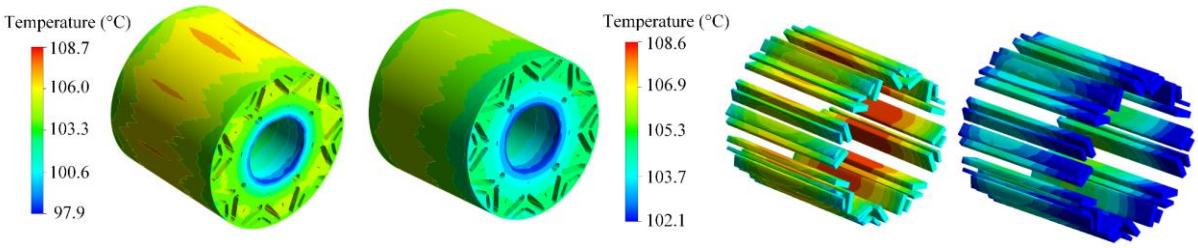


(e) (f) (g) (h)

**Fig. 8 Temperature field of motor at rated speed. (a) Stator core of IM.(b) Stator core of OM. (c) Winding of IM.(d) Winding of OM. (e) Rotor core of IM. (f) Rotor core of OM. (g) PM of IM. (h) PM of OM.**

## 5. Conclusion

In order to solve the problem of uneven flow on both sides in the oil-cooling PMSM, the rotational oil-spray-cooling structure is optimized in this paper. An optimization method combining the Taguchi method and the response surface method is used to optimize the structure. The fluid field and temperature field under the rated working condition of the motor before and after optimization are compared and analyzed, and the following conclusions are obtained.

1) Using the combination method to optimize the oil-spray-cooling structure, the important variables can be quickly determined. The structural parameters of the shaft have an important role in the uniform cooling of the motor. And the parameters A, C and D have a significant influence on the temperature of motor.
2) By comparing the fluid field before and after optimization under the rated working condition, the optimized motor can distribute the oil to both sides. And the oil is distributed in the cavities on both sides of the motor, which indicates the effectiveness of the optimization method.
3) The temperature field of the initial model and the optimization model at the rated working condition are calculated. The maximum temperature of the rotor is reduced by 3 °C, the temperature difference of the winding is reduced by 2 °C, and the maximum temperature does not increase. It indicates that the optimized oil-spray-cooling structure can provide greater cooling performance under the same oil supply conditions.

## References

[1] A. Miyamoto, *et al*., Automatic model order reduction technique for real-time temperature monitoring of oil-cooled electric machines, *IEEE Transactions on Industry Applications*, 60 (2024),1, pp. 477-485

[2] Xie, Y., *et al*. Design and optimisation of oil injection pipe cooling structure for permanent magnet synchronous motors in hybrid electric vehicles. *IET Electr. Power Appl.* 18 (2024),3, pp. 345-355

[3] C. Liu, *et al*., Experimental investigation of oil jet cooling in electrical machines with hairpin windings, *IEEE Transactions on Transportation Electrification*, 9 (2023),1, pp. 598-608

[4] Jiacheng Zhang, Baojun Ge, Design and thermal performance analysis of a new water-cooled structure for permanent magnet synchronous motors for electric vehicles, *Therm. Sci.* Vol. 27, (2023) No. 3B, pp. 2423-2432.

[5] P. Liang, *et al*., Water jacket and slot optimization of a water-cooling permanent magnet synchronous in-wheel motor, *IEEE Transactions on Industry Applications*, 57 (2021),3, pp. 2431-2439

[6] An Zhao, *et al*., Parameter study for oil spray cooling on endwindings of electric machines via eulerian–lagrangian simulation, *Applied Thermal Engineering*, 235(2023), pp.121281.

[7] C. Liu, *et al*., Estimation of oil spray cooling heat transfer coefficients on hairpin windings with reduced-parameter models, *IEEE Transactions on Transportation Electrification*, 7(2021),2, pp. 793-803

[8] H. Wang, *et al*., Oil injection cooling design for the ipmsm applied in electric vehicles, *IEEE Transactions on Transportation Electrification*, 8(2022),3, pp. 3427-3440

[9] Z. Song, *et al*., An improved dual iterative transient thermal network model for PMSM with natural air cooling, *IEEE Transactions on Energy Conversion*, 37(2022),4, pp. 2588-2600

[10] D. Liang, *et al*., Tracking of winding and magnet hotspots in spmsms based on synergized lumped-parameter and sub-domain thermal models, *IEEE Transactions on Energy Conversion*, 37(2022),3, pp. 2147-2161

[11] Y. Tang, *et al*., Investigation of open-circuit fault-tolerant strategy in a modular permanent magnet synchronous in-wheel motor based on electromagnetic–thermal analysis, *IEEE Transactions on Transportation Electrification*, 8(2022),1, pp. 1085-1093

[12] S. S. Pasunurthi, *et al*., 3-D CFD simulation of oil flow and heat transfer in an electric drive unit, *2023 IEEE International Transportation Electrification Conference* (ITEC-India), Chennai, India, 2023, pp. 1-9

[13] P. Lindh, *et al*., Two cooling approaches of an electrohydraulic energy converter for non-road mobile machinery, *IEEE Transactions on Industry Applications*, 59(2023),1, pp. 736-744

[14] S. K. Sunori, *et al*., Torque optimization of a synchronous motor using a genetic algorithm, *2023 7th International Conference on Electronics, Communication and Aerospace Technology* (ICECA), Coimbatore, India, 2023, pp. 17-21.

[15] M. Amaidi and A. Mansouri, Genetic Algorithm based Multi-objective optimization of SMPM, *2023 20th International Multi-Conference on Systems, Signals & Devices* (SSD), Mahdia, Tunisia, 2023, pp. 633-636.

[16] W. Zhao, *et al*., Multiobjective optimization of a double-side linear vernier pm motor using response surface method and differential evolution, *IEEE Transactions on Industrial Electronics*, 67(2020),1, pp. 80-90

[17] W. Hu, *et al*., Optimization of cogging torque of permanent magnet-assisted synchronous reluctance motor based on improved taguchi method, *2023 6th International Conference on Electrical Engineering and Green Energy* (CEEGE), Grimstad, Norway, 2023, pp. 124-129

[18] K. Li, *et al*., Multi-objective optimization of concentrated flux interior permanent magnet in-wheel motor with distributed winding, *2023 26th International Conference on Electrical Machines and Systems* (ICEMS), Zhuhai, China, 2023, pp. 579-584

[19] L. Wang, *et al*., Research on coupling heat transfer of fluid and solid under rotating state of water-cooled permanent magnet synchronous motor for compressor, *Proceedings of the CSEE*, 41(2021),22, pp.7830-7840

[20] Xie, Y., *et al*., The relationship study between field changes and faulty condition in squirrel-cage induction motor with broken bars fault, *Proceedings of the CSEE*, 37(2017),14, pp. 4222-4231

[21] C.W. Hirt, B.D. Nichols, Volume of fluid (VOF) method for the dynamics of free boundaries, *J.*

*Comput. Phys.* 39 (1981),1, pp. 201-225

[22] Li W., *et al.*, Stator-rotor coupled thermal field numerical calculation of induction motors and correlated factors sensitivity analysis. *Proceedings of the CSEE*, 27(2007), 24, pp.85-91

[23] Fan X., *et al.*, Water cold plates for efficient cooling: verified on a permanent-magnet machine with concentrated winding. *IEEE Transactions on Industrial Electronics*,67(2020),7, pp.5325-5336

Submitted: 30.03.2024.
Revised: 25.06.2024.
Accepted: 27.06.2024